Optics Letters

Selective terahertz absorber for angle and polarization-independent spectral sensing

Christopher Arose,[1] Anthony C. Terracciano,[2,3] Robert E. Peale,[1,4] and Subith S. Vasu[2,3,4,*]

[1]Department of Physics, University of Central Florida (UCF), 4000 Central Florida Blvd, Orlando, Florida 32816, USA
[2]Department of Mechanical and Aerospace Engineering, University of Central Florida, 4000 Central Florida Blvd, Orlando, Florida 32816, USA
[3]Center for Advanced Turbomachinery and Energy Research (CATER), University of Central Florida, 4000 Central Florida Blvd, Orlando, Florida 32816, USA
[4]CREOL, the College of Optics and Photonics, University of Central Florida, 4000 Central Florida Blvd, Orlando, Florida 32816, USA
*Corresponding author: subith@ucf.edu

Received 22 November 2021; revised 1 February 2022; accepted 13 February 2022; posted 15 February 2022; published 14 March 2022

Polarization- and incident-angle-independent narrow-band terahertz (THz) absorbers were developed to enable THz imaging, radar, and spectroscopy applications. The design comprises a transparent fused silica (SiO_x) substrate backed by an optically thick metal layer and topped by a periodic array of metal cross patterns. Finite element analysis (FEA) simulations optimized the geometry of devices fabricated by contact photolithography. Resonances were characterized by Fourier-transform reflectance spectroscopy. The design tunable absorption bands appeared in the range 50–200 cm^{-1} (1.5–6 THz) with full widths at half maximum of 20–56 cm^{-1} (0.6–1.68 THz). Maximum absorption was −8.5 to −16.8 dB. The absorption bands are independent of incidence angle and polarization in agreement with simulation.

https://doi.org/10.1364/OL.449308

The terahertz (THz) region of the electromagnetic spectrum (0.1 THz to 10 THz) has applications in imaging, telecommunications, and spectroscopy, which would be enabled by advances in THz detector technology. The THz spectral filters based on selectively resonant structures and frequency-selective surfaces can provide band-stop filtering for removing spurious signals in many applications, including the fabrication of monochromatic laser systems [1–3]. However, many of these filtering techniques, such as metal patches and split-ring resonators (SRRs), introduce some degree of polarization or incident angle dependence [4–6]. Here we demonstrate a reflective band-stop filter for this spectral region that is largely independent of both polarization and incident angle.

The many suggestions for spanning the "THz Gap" with novel detectors and sources [7–13] require simultaneous advances in spectral filters and wavelength-selective absorbers. Resonant absorbers are needed to enable wavelength-selective thermal detectors, including pyroelectric, thermopile, and bolometer types [14]. Polarization and incident angle insensitivity would be advantageous in waveguide systems.

Approaches include frequency-selective surfaces comprising arrays of subwavelength resonant structures. Frequency selective surfaces that provide band-stop filtering have taken many forms as applied to radio and infrared (IR) frequencies [6,15–20]. These surfaces include Salisbury screens, SRRs, metal patches, and hole arrays in otherwise continuous metal films. Plasmonic resonances are used to create spectrally selective absorbers in films of negligible thickness compared to transverse structure dimensions, which are themselves smaller than the operating wavelength [21–23]. They may be considered either a metamaterial with effective optical constants or a collection of independent resonators. Geometry and material properties define the resonances. These absorbers can be used to create spectrally selective thermal detectors [24–27], such as pyroelectrics and bolometers. Here, we extend the approach to the far-IR/THz region.

Some published absorber designs are asymmetric, which causes absorption to depend on polarization and incidence angle [4–6]. A possible solution is using symmetric absorber designs [16].

The resonant absorber considered here was adapted from our initial investigations [27,28]. Patterning was achieved by contact photolithography onto a dual-sided polished (DSP) 500-μm-thick (Z dimension) fused silica wafer. The symmetry in the plane is that of a square. An optically thick Au-film was deposited on a Ti sticking layer by electron beam evaporation for a total thickness of 100 nm. The patterned surface metal was of the same construction. The absorber pattern was periodically repeated to fill ~360 mm^2 of the wafer. Figure 1 presents a schematic of one unit cell for the surface pattern. The critical dimensions are the periodicity W, the spacing between the inner and outer cross t, and the width of the inner cross t1.

Figure 2 presents spectra for the IR index n and extinction coefficient κ for fused silica [29]. The dispersion is smooth. Strong isolated dispersion features have been shown to give rise to unintended resonances [30], but such are lacking here. Thus, we expect any resonances below 6 THz to be determined mainly by the design geometry. Figure 2 also presents the far-IR complex index spectrum for gold.

No sharp features that might lead to parasitic resonances are present. Simulations were performed in CST Studio Suite 2019 (3DS Dassault Systems) high-frequency 3D simulation package

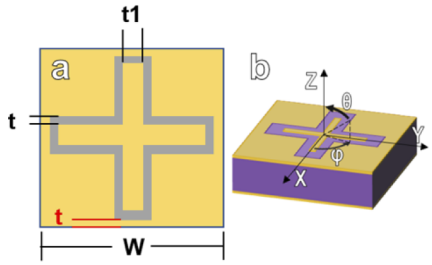

Fig. 1. (a) Schematic of the absorber unit cell with critical dimensions labeled. (b) Off-axis view of the layer stack.

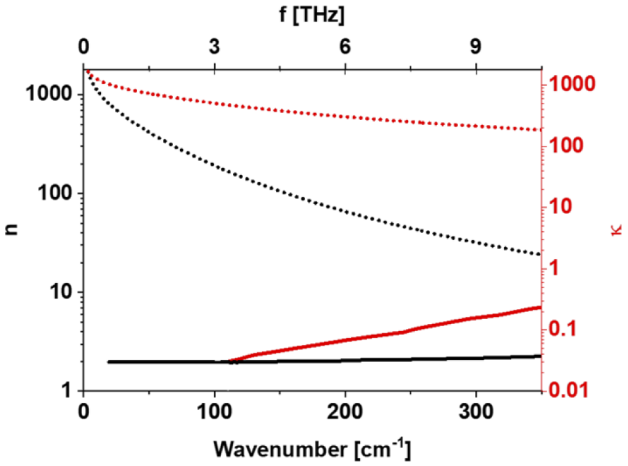

Fig. 2. THz refractive index of fused silica (solid) [29], THz refractive index of gold (dotted) [4].

utilizing finite element analysis (FEA). A Drude permittivity is assumed for gold, while a Lorentzian model with parameters from Refs. [4,29] was used for silica. Periodic boundary conditions were used in the plane. The far-field boundary was placed at least 25 μm above and parallel to the surface. Nearest-neighbor averaging reduced Fabry–Pérot artifacts.

Reflectance spectra were obtained using vacuum-bench Fourier spectrometer (Bomem DA8) at 8-cm^{-1} resolution [31]. A 3X-beam condenser and spectral reflectance accessory (Perkin-Elmer) were used to measure near-normal (8°) incidence. The variable angle reflectance accessory (Agilent) permitted incidence angles from 20° to 60°. A gold mirror was used for reference. Reflectance was calculated as the ratio of sample to reference reflected power. A wire-grid on polyethylene far-IR polarizer was used for polarization studies.

Figure 3 presents unpolarized simulated and measured reflectance spectra R at near-normal incidence for six samples, whose geometrical parameter values are given in Table 1. The periodic ripples in the simulated spectra are identified by their period as due to Fabry–Pérot resonances in the substrate, which are unresolved in the experiment. The inset in Fig. 3 is an example of the field distribution at resonance. The rate of heat dissipation for monochromatic light per unit volume is $\frac{\omega}{8\pi}\varepsilon''|E|^2$, where $\varepsilon'' = 2n\kappa$ is the imaginary part of the permittivity [32]. Assuming the field penetrates the Au by the skin depth ~30 nm, that it is reduced thereby the ratio of skin depth to wavelength, and that the fields are uniform over the volumes they penetrate, we estimate that the rate of heat generation in one unit cell is 7 orders higher in the dielectric than in the gold

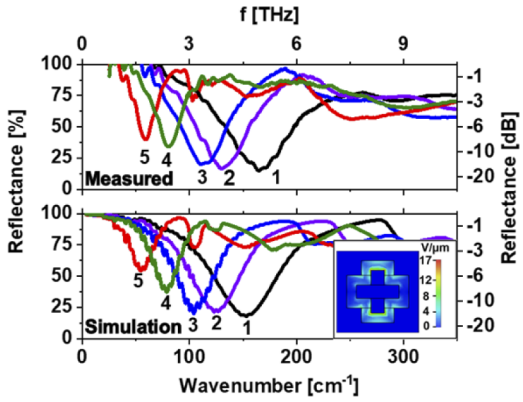

Fig. 3. Unpolarized normal incidence reflectance spectra, simulation, and experiment. Absorption = 1 − R. (Inset) Simulated electric field distribution for Sample 1.

Table 1. Key Filter Properties

Sample	W/μm	t/μm	t1/μm
1	25	3	4
2	30	3.5	4
3	35	4	4.5
4	40	3	2
5	45	2.5	4

Sample	*Q*-factor		Centerline/THz		Reflectance Min/dB	
	Meas	Sim	Meas	Sim	Meas	Sim
1	2.8	2.2	5.0	4.6	−17	−15
2	2.4	2.2	3.9	3.8	−16	−13
3	2.2	2.3	3.4	3.1	−14	−13
4	3.2	2.9	2.5	2.4	−10	−8.0
5	2.9	1.9	1.7	1.7	−8.5	−5.4

at 6 THz. This holds even though the dielectric is much less lossy than the metal. In other words, the metal structures serve to concentrate fields in the dielectric, where the electromagnetic energy is dissipated.

The maximum difference in resonance frequency is 8% (Sample 4). Absorption 1 − R increases monotonically with resonance frequency with a maximum difference of 1 dB. Device performance parameters are collected in Table 1. All Q = f/Δf values exceed ½, so the resonances are underdamped as desired for high selectivity. The resonances are clearly design tunable. As the periodicity W increases, the absorption frequency redshifts as expected [33].

Figure 4 presents polarization dependence for normal incidence on Sample 1. Peak values are polarization-independent, which is verified by the simulated reflectance spectrum in Fig. 4(a), where all curves coincide. Figure 4(b) presents the measured reflectance spectra with more minor polarization effects than the ~5% experimental uncertainty.

Figure 5 presents dependence on the angle of incidence for Sample 1. Simulation results in Fig. 5 are split into the TE and TM modes, where we see differences in behavior with increasing angles. In particular, absorption decreases as the TE polarization angle increases, and both modes exhibited a small redshift. The uncertainties in the unpolarized experiment with the variable angle accessory were too large to observe these changes.

In summary, a thin-film wavelength-selective absorber comprising a periodically cross pattern on silica on continuous metal

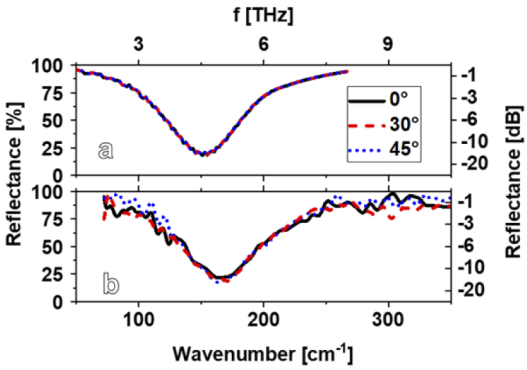

Fig. 4. Polarization dependence for Sample 1. (a) Simulated and (b) measured reflectance spectra.

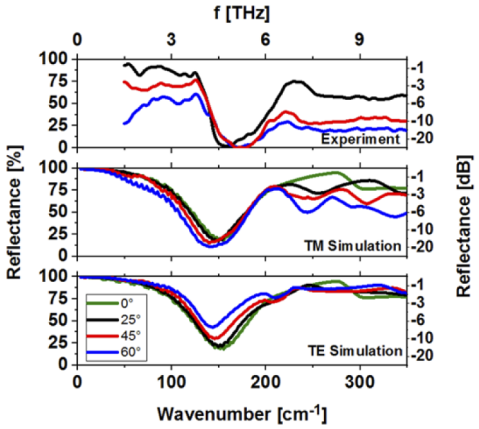

Fig. 5. Effect of incidence angle.

was designed, fabricated, and characterized. The largest FWHM of 56 cm^{-1} (1.68 THz) had ~86% absorption at 5-THz center frequency. The narrowest peak had a FWHM of 20 cm^{-1} (0.6 THz) with the absorption of ~61% at 1.7 THz. The absorption bands were independent of incidence angle up to 60° and were independent of polarization. Such absorbers would be useful as band-blocking filters on curved surfaces such as focusing mirrors used in spectroscopy or laser applications.

Funding. National Aeronautics and Space Administration (80NSSC20M0093, 80NSSC21K1901); Defense Advanced Research Projects Agency (D18AP00040).

Disclosures. The authors declare no conflicts of interest.

Data availability. Data underlying the results presented in this paper are not publicly available at this time but may be obtained from the authors upon reasonable request.

REFERENCES

1. K.R. Armstrong and F.J. Low, Appl. Opt. **13**, 425 (1974).
2. K.J. Leiptoldt, T. Happich, E. Kreysa, and H.P. Gemund, Int. J. Infrared Millimeter Waves **12**, 263 (1991).
3. R. Szipocs, A. Kohazi-Kis, P. Apai, E. Finger, A. Euteneuer, and M. Hofmann, Appl. Phys. Lett. B **70**, S63 (2000).
4. A. Derkachova, K. Solwas, and I. Demchenko, Plasmonics **11**, 941 (2016).
5. A. Datta, Z. Zeng, and X. Xu, Opt. Express **27**, 28264 (2019).
6. J. Le Perchec, R. E. Lamaestre, M. Brun, N. Rochat, O. Gravrand, G. Badano, J. Hazart, and S. Nicoletti, Opt. Express **19**, 15720 (2011).
7. J. Wang, J. Gou, and W. Li, AIP Adv. **4**, 027106 (2014).
8. W.D. Zhang, A. Bykhovski, L.S. Himed, and E.R. Brown, in *IEEE National Aerospace and Electronics Conference* (IEEE, 2019).
9. G. Ducournau, Nat. Photonics **12**, 574 (2018).
10. A. Ebrahimi, R.T. Ako, W.S.L. Lee, M. Bhaskaran, S. Sriram, and W. Withayachumnankul, IEEE Trans. Terahertz Sci. Technol. **10**, 204 (2020).
11. S. Barzegar-Parizi, A. Ebrahimi, and K. Ghorbani, Opt. Laser Technol. **132**, 106483 (2020).
12. A. Ebrahimi and S. Barzegar-Parizi, J. Opt. Soc. Am. B **37**, 2372 (2020).
13. A. Ebrahimi and S. Barzegar-Parizi, Electronics **10**, 1860 (2021).
14. E. M. Smith, J. Nath, J. Gin III, R. E. Peale, and D. Shelton, in SPIE Defense and Security (SPIE, 2016).
15. J. Cunningham, C. Wood, A. G. Davies, I. Hunter, E. H. Linfield, and H. E. Beere, Appl. Phys. Lett. **86**, 213503 (2005).
16. D. Zhai, R. Zhao, Z. Geng, B. Cui, and Y. Yang, Proc. SPIE **10826**, 1082613 (2018).
17. R.L. Fante and M.T. McCormack, IEEE Trans. Antennas Propag. **36**, 1443 (1988).
18. A. N. Reddy and S. Raghavan, IEEE International Conference On Emerging Trends in Computing, Communication, and Nanotechnology (IEEE, 2013).
19. J. H. Goldsmith, S. Vangala, J. R. Hendrickson, J. W. Cleary, and J. H. Vella, J. Opt. Soc. Am. **34**, 1965 (2017).
20. J. Nath, S. Modak, I. Rezadad, D. Panjwani, F. Rezaie, J. W. Cleary, and R. E. Peale, Opt. Express **23**, 20366 (2015).
21. J. Talghader, A. Gawarikar, and R. Shea, Light: Sci. Appl. **1**, e24 (2012).
22. T. Ebbesen, H. Lezec, H. Ghaemi, T. Thio, and P. A. Wolff, Nature **391**, 667 (1998).
23. B. Wang, L. Wang, G. Wang, W. Huang, X. Li, and X. Zhai, IEEE Photonics Technol. Lett. **26**, 111 (2014).
24. T. D. Dao, S. Ishii, T. Yokoyama, T. Sawada, R. P. Sugavaneshwar, K. Chen, Y. Wada, T. Nabatame, and T. Nagao, ACS Photonics **3**, 1271 (2016).
25. H. Tao, C. M. Bingham, D. Pilon, K. Fan, A. C. Strikwerda, D. Shrekenhamer, W. J. Padilla, X. Zhang, and R. D. Averitt, J. Phys. D: Appl. Phys. **43**, 225102 (2010).
26. S. Ghosh and K. V. Srivastava, IEEE Trans. Antennas Propag. **64**, 3665 (2016).
27. A.C. Terracciano, S. S. Vasu, C. Arose, and R.E. Peale, "Ultra-spectrally selective THZ pyroelectric detector," U. S. patent application 17/228,801 (13April2020).
28. A. C. Terracciano, S. S. Vasu, and C. Arose, "Ultra-spectrally selective THz band stop reflector," U. S. patent application 17 / 456,493 (24November2021).
29. R. Kitamura, L. Pilon, and M. Jonasz, Appl. Opt. **46**, 8118 (2007).
30. R.N. Evans, S.R. Calhoun, J.R. Brescia, J.W. Cleary, E.M. Smith, and R.E. Peale, MRS Adv. **4**, 667 (2019).
31. B. Köroğlu, J. Quant. Spectrosc. Radiat. Transfer **152**, 107 (2015).
32. L.D. Landau, E.M. Lifshitz, and L. P. Pietaevskii, *Electrodynamics of Continuous Media*, 2nd ed. (Elsevier, 1984), section 80.
33. D. Sadrid and A. Challener, *Modern Introduction to Surface Plasmons: Theory, Mathematica Modeling, and Applications* (Cambridge University Press, 2010).